JACS Au
AN OPEN ACCESS JOURNAL OF THE AMERICAN CHEMICAL SOCIETY

pubs.acs.org/jacsau

Article

Achieving Ultrasensitive Chromogenic Probes for Rapid, Direct Detection of Carbapenemase-Producing Bacteria in Sputum

Wenshuai Li, Jingjing Wang, Chen Li, Zhiyou Zong, Jinzhong Zhao, Hongmei Gao, and Dingbin Liu*

Cite This: *JACS Au* 2023, 3, 227−238

Read Online

ACCESS | Metrics & More | Article Recommendations | Supporting Information

ABSTRACT: Carbapenemase-producing bacteria (CPB) stand as the most dangerous "superbugs" in the clinic. Rapid point-of-care (POC) detection of CPB in clinical samples is key to timely and effective infection management. We herein report the first ultrasensitive chromogenic probe that allows direct POC detection of CPB in clinical sputum samples at a sample-to-result time of less than 15 min. This chromogenic probe is modularly designed by conjugating the carbapenem core with a benzene derivative bearing an electronegativity-tunable substituent. Unexpectedly high sensitivity was achieved simply by choosing strong electron-withdrawing substituents, such as $-N^{+}(CH_3)_3$, without resorting to complex molecular design. Through integrating the probes with a portable paper chip, 24 out of 80 clinical sputum samples from sepsis patients with lung infections were quickly diagnosed as CPB-positive, exhibiting 100% clinical sensitivity and specificity. This low-cost paper chip assay can be readily performed on-site, breaking through the dilemma of rapid CPB detection, especially in resource-limited settings.

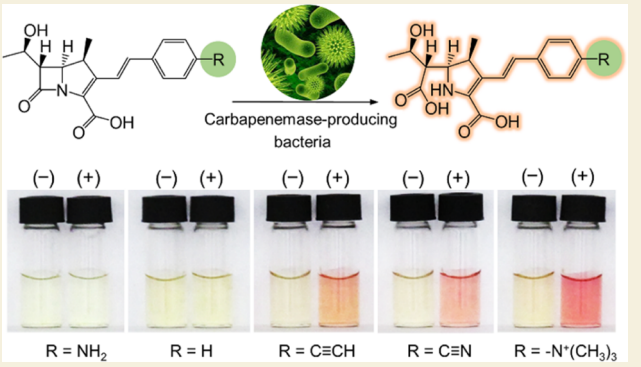

KEYWORDS: *carbapenemase-producing bacteria, antibiotic resistance, chromogenic probe, POC detection, paper chip*

INTRODUCTION

Antimicrobial resistance has become a major global threat to public health.[1] The inappropriate use of antibiotics in both medicine and agriculture has accelerated the spread of antibiotic-resistant bacteria, causing the emergence of "superbugs".[2] Among the commonly used antibiotics, carbapenems are the most potent broad-spectrum antibiotics against both Gram-positive and Gram-negative bacteria and have thus been recognized as the last-resort drugs in treating serious bacterial infections.[3] Unfortunately, carbapenem resistance in bacteria has become increasingly prevalent worldwide due to the emergence and rapid spread of carbapenemases across different pathogenic species.[4] Therefore, carbapenemase-producing bacteria (CPB) have become the leading cause of therapeutic failure of bacterial infections in both hospital and community settings.[5] Effective infection management thus calls for rapid point-of-care (POC) detection of CPB in clinical samples to facilitate timely and appropriate prescription and improve patient outcomes.

Currently, culture-based assays act as the gold standard for identifying antibiotic-resistant bacteria.[6] These assays, however, are based on bacterial growth that often requires a minimum of 24 h of sample culture.[7] In some cases, such as bacteremia and sepsis, the sample culture requires several days to weeks.[8] In clinical practice, clinicians often prescribe a hefty dose of broad-spectrum antibiotics empirically to treat an unknown infection before they obtain the diagnostic results from culture, leading to overuse and sometimes misuse of antibiotics.[9] Other approaches have been developed to shorten the diagnosis time, such as real-time polymerase chain reaction (RT-PCR),[10] gene sequencing,[11] mass spectrometry,[12] optical detection,[13−20] thermal measurement,[21] nanomechanical sensing by cantilevers,[22] and plasmonic nanosensors.[23] Most of these methods require expensive equipment, skilled personnel, or/and complex sample processing (e.g., cell lysis, nucleic acid extraction, sample purification, and signal amplification) and thus cannot be used outside of a laboratory setting. Hence, developing simple assays for rapid and direct identification of CPB in real clinically relevant samples is urgently desired but has not been achieved yet.

Over the past decades, chromogenic probes based on target-activated color change have been widely used to design POC assays.[24] A classical one is nitrocefin, which can be hydrolyzed by β-lactamases to result in a distinct yellow-to-red color change, allowing rapid detection of β-lactamases by the naked

Received: November 8, 2022
Revised: December 12, 2022
Accepted: December 16, 2022
Published: December 27, 2022

https://doi.org/10.1021/jacsau.2c00607
JACS Au 2023, 3, 227−238

eye.[25] However, the nitrocefin-based assay is unable to discriminate subtypes of β-lactamases and thus lacks specificity to detect carbapenemases. Carba NP testing is the only carbapenemase-specific chromogenic assay that has been approved by the Clinical and Laboratory Standards Institute (CLSI).[26,27] Although this assay can deliver a result in 2 h nominally, it suffers from low sensitivity, thus offering false-negative results.

Herein, we achieved the first ultrasensitive carbapenemase probe based on the chromogenic carbapenem substrate (CCS) that could directly readout the presence of CPB in clinical sputum by a color change in less than 15 min. Different from previously reported carbapenemase-specific molecular probes that rely on conjugating the carbapenem core with a fluorophore or luminescent reporter,[16−20] the structure of CCS appears to be simpler—only by extending the π-conjugation of the carbapenem core with a benzene derivative bearing an electronegativity-tunable substituent. Unexpectedly, we discovered that the chromogenic property of CCS can be fine-tuned by the substituent, and its sensitivity is proportional to the substituent's electron-withdrawing capability. By choosing a strongly electron-withdrawing substituent such as $-N^+(CH_3)_3$, the detection limits for clinical CPB isolates can be down to 10^4 CFU/mL level, 3 orders of magnitude lower than that of the currently used chromogenic Carba NP assay. When CCS-$N^+(CH_3)_3$ was integrated with a portable and easy-to-use paper chip, the CPB in the sputum of lung-infected patients was quickly detected, without resorting to any instruments, skilled operators, costly reagents, and complex procedures. 24 out of 80 cases were diagnosed with carbapenem-antibiotic resistance, exhibiting 100% clinical sensitivity and specificity, as validated by RT-PCR and culture-based assays. Given the simplicity, low cost, high speed, and high accuracy, the CCS-based assay potentiates translational implications for POC detection of CPB in diverse settings.

EXPERIMENTAL METHODS

Fabrication of Paper Chips for the Assay

The production process of the paper chips includes four steps: pattern design, engraving seal, waxing, and printing. Briefly, we used CAD software to design a chip by setting a circular hydrophilic zone with 3 mm diameter in the center of a 12 mm × 6 mm hydrophobic wax layer. Next, a seal with the designed pattern was carved on a high-temperature resistant plate. Then, the paraffin was melted evenly on the surfaces of the engraved seal, which was finally transferred to a Whatman grade filter paper to form a chip with hydrophobic barriers. 5 μL of 2.0 mM of CCS-$N^+(CH_3)_3$ dissolved in chloroform was dropped into a closed round hole and dried at room temperature overnight prior to use.

Gene Synthesis, Plasmid Construction, and Bacterial Strains

Through searching the National Center for Biotechnology Information (NCBI) website (https://www.ncbi.nlm.nih.gov/), we obtained both the genetic and amino acid sequences of 11 β-lactamases, including 5 carbapenemases NDM-1, IMP-4, KPC-3, VIM-27, and OXA-48; 3 extended-spectrum β-lactamases (ESBL) SHV-5, TEM-7, and CTX-M-3; 2 AmpC β-lactamases (AmpC) MOX-1 and CMY-4; and 1 broad-spectrum β-lactamase (BSBL) TEM-1. 11 recombinant *Escherichia coli* BL21 (DE3) of β-lactamase genes were purchased from Sangon Biotech (Shanghai) for protein expression. We first submitted the DNA and protein sequences for codon optimization and whole-gene synthesis. We then selected the Bamhi and Xhol restriction sites to introduce the corresponding genes into pET-28a (+) plasmid vectors, where the 5′ end of target gene was His_6-tagged. Finally, the recombinant plasmids were transformed into *E. coli* BL21 (DE3) by the heat shock method and screened in solid Luria−Bertani (LB) medium with 50 μg/mL kanamycin.

Production and Purification of β-Lactamases

The screened *E. coli* BL21 (DE3) was cultured in 1 L of liquid LB medium containing 100 μg/mL kanamycin at 37 °C until the optical density at 600 nm (OD_{600}) reached 0.3−0.5. β-Lactamases were overexpressed by the addition of 0.5 mM isopropyl-6 β-D-thiogalactopyranoside under shaking at 30 °C overnight. Bacteria were first collected by centrifugation and resuspended in a lysis buffer containing 300 mM NaCl, 50 mM Tris−HCl (pH 7.4), 1 mM phenylmethanesulfonyl fluoride, and 2 mM dithiothreitol. The resuspended solution was treated using a Biospec MiniBeadBeater-96 cell disrupter for 10 min and finally centrifuged to remove the cell debris at 4 °C. The supernatant was filtered through a 0.45 μm hydrophilic membrane, followed by incubating with the Ni-NTA agarose (Novagen) in the recombinant protein column. To remove the foreign proteins, the column was progressively rinsed with the mixtures of 20 mM *N*-(2-hydroxyethyl)piperazine-*N*′-(2-ethanesulfonic acid) (HEPES) buffer (pH 7.4) and 0.5 M NaCl containing 5, 10, and 20 mM imidazole. Subsequently, gradient concentrations (from 100 mM to 400 mM over 120 min, 3 mL/min) of imidazole were dissolved in the mixture of 20 mM HEPES buffer (pH 7.4) and 0.5 M NaCl as the eluent to release the target His_6-tagged proteins from the column. A rapid detection test strip was used to monitor the entire protein elution process. The target proteins (3 mL) were collected at about 80 min under the elution of 300 mM imidazole. The crude products were dialyzed in 1 L of the mixture of 20 mM HEPES buffer (pH 7.4) and 0.5 M NaCl for 9 h with a buffer change every 3 h, followed by concentrating with a 10 kDa protein concentrator. The concentrates were then resuspended in 1 mL of the solution containing 20 mM HEPES buffer (pH 7.4) and 0.15 M NaCl. Ultimately, we employed Sangon Biotech (Shanghai) to further purify the achieved proteins using gel filtration chromatography. In short, a Sephadex G-100 column (4−150 kDa, 1.2 × 70 cm) was first equilibrated with the mixture of 20 mM HEPES buffer (pH 7.4) and 0.25 M NaCl using the PPS−HD protein chromatography system. Then, 1 mL of the crude target protein was diluted with 9 mL of the mixture of 20 mM HEPES buffer (pH 7.4) and 0.25 M NaCl. The resulting solution was filtered and subjected to the gel filtration on the Sephadex G-100 column at 4 °C. The column was washed with the same buffer at a flow rate of 2 mL/min. The proteins were measured at an absorbance of 280 nm and fractionated for collection, while their sizes were determined by sodium dodecyl sulfate polyacrylamide gel electrophoresis (SDS-PAGE). The target proteins were concentrated using 10 kDa protein concentrators and then resuspended in 1 mL of the storage buffer containing 20 mM HEPES, 0.15 M NaCl, and 20% glycerol. Finally, the target recombinant proteins of β-lactamases were determined by a bicinchoninic acid assay and stored at −80 °C for further use.

Identification of Recombinant Proteins by SDS-PAGE

70 μL of double-distilled H_2O (ddH_2O) was added to the mixture of 20 μL of SDS-loading buffer (6×) and 30 μL of protein sample, which was heated in a 100 °C water bath for 20 min. After that, the resulting solution was centrifuged at 8000 r/min for 3 min and the supernatant was subjected to SDS-PAGE. 20 μL of protein mixture and 5 μL of color-mixed protein marker (BeyoGel, 15−130 kDa) were added to BeyoGel SDS-PAGE pregel (Tris−Gly, 15%, 12 wells). The voltage was set to 120 V, and the electrophoresis time was 20−30 min. The electrophoresis buffer (Tris−Gly) was prepared by dissolving 3.03 g of tris(hydroxymethyl)methyl aminomethane THAM (Tris), 18.8 g of glycine (Gly), and 1 g of SDS into 1 L of ddH_2O. After electrophoresis, the polyacrylamide gel was washed with ddH_2O, followed by soaking in a Coomassie brilliant blue solution at 25 °C for 2 h, and finally decolorized by the decolorization solution composed of 30 mL of methanol, 10 mL of acetic acid, and 60 mL of ddH_2O. The Coomassie brilliant blue solution was prepared by dissolving

https://doi.org/10.1021/jacsau.2c00607
JACS Au 2023, 3, 227−238

0.125 g of Coomassie brilliant blue R-250 in the decolorization reagent.

Liquid Chromatography–Mass Spectrometry Analysis of CCSs and their Hydrolyzed Products

A Shimadzu liquid chromatography–mass spectrometry (LC–MS) system equipped with an LC-20AT gradient pump and an online diode UV–vis detector was used for determining the molecular weights. The chromatographic column type used was ShimNex WR C18, 4.6 × 250 mm, 5 μm; the column temperature was 25 °C; the sample concentration was 1 μM; the injection volume was 50 μL; the flow rate was 1 mL/min; the detection wavelength was 254 nm; mobile phases A and B were MeCN and 0.1% trifluoroacetic acid solution, respectively; and the running time was 40 min.

Docking Details

The crystal structure of NDM-1 (PDB code: 6TGD) was obtained from the protein data bank (PDB). The structures of five CCSs were drawn by ChemDraw 19.0. All CCSs are fully flexible in the docking process, while the active area of NDM-1 is semi-flexible in refinement. The histidine residues of NDM-1 were protonated based on their calculated pK_a values. The enzyme-HADDOCK allowed CCS dockings in water equilibration. The docking process went through three steps: (i) rigid-body docking was used for quick screening for each assembly; (ii) 200 structures were selected from the 1000 rigid-body docking complexes for the subsequent semi-flexible refinement; and (iii) a short molecular dynamics simulation was employed to refine the docking models in an explicit solvent. Then, a maximum of 200 docking models for each assembly was clustered and analyzed based on van der Waals forces, electrostatic energy, and desolvation. The optimal binding pose for each enzyme–CCS system was obtained from their best cluster. PRODIGY was employed to calculate the binding affinity of NDM-1 with the five CCSs based on their optimal docking structures.

Determination of Detection Limits of CCSs

Aliquots of CCSs (R = $-N^+(CH_3)_3$, $-C{\equiv}N$, or $-C{\equiv}CH$, 1 μL, 1 mM) were incubated with 100 μL of various concentrations (0, 10, 25, 50, 100, 200, and 300 pM) of carbapenemases (NDM-1, IMP-4, KPC-3, VIM-27, and OXA-48) in pH 7.4 PBS at 37 °C for 30 min. The incubation was performed in a sterile 96-well microplate, and the absorbance at 591 nm (A_{591}) was monitored during the incubation by a microplate reader. The A_{591} values versus the concentrations of carbapenemases were fitted to specific calibration curves to obtain the slopes k. The detection limits of NDM-1, IMP-4, KPC-3, VIM-27, and OXA-48 were calculated on the basis of $3S/k$, where S is the standard deviation of six parallel blank samples.

Determination of the Molar Extinction Coefficient of CCS-$N^+(CH_3)_3$

Diverse concentrations of CCS-$N^+(CH_3)_3$ (0.04, 0.19, 0.37, 0.74, 1.86, 3.71, and 5.57 mg/L) were first dissolved in PBS (pH 7.4). Then, their absorbance at 417 nm (A_{417}) was recorded in a 96-well microplate at 37 °C. Three separate replications were carried out to ensure the result reliability. A linear relationship was generated by graph fitting using the substrate concentration as the X axis and the absorbance as the Y axis. The molar extinction coefficient of CCS-$N^+(CH_3)_3$ was calculated according to the Lambert–Beer law: $A = \varepsilon bc$ (where b is the optical path length, c is the concentration of the light-absorbing substance, and ε is the extinction coefficient). Three replicates of parallel samples were tested to offer the standard deviations.

Inhibition Tests of CCS-$N^+(CH_3)_3$ Hydrolysis

Aliquots of phenylboronic acid (PBA) or ethylenediaminetetraacetic acid (EDTA) (1 μL, 1 M) were incubated with 500 μL of carbapenemases (NDM-1, IMP-4, KPC-3, VIM-27, and OXA-48, 3 nM) in pH 7.4 PBS at 37 °C for 10 min. The mixtures were added with 500 μL of CCS-$N^+(CH_3)_3$ (20 μM). The resulting solutions were maintained for 30 min at 37 °C. The absorbance of the solutions at 591 nm (A_{591}) was monitored by a microplate reader during the incubation. Three replicates of parallel samples were tested to offer the standard deviations.

Carbapenemase Kinetics

We determined the kinetic data of carbapenemases by the Michaelis–Menten model. Aliquots of five carbapenemases (0.2 nM), including NDM-1, IMP-4, KPC-3, VIM-27, and OXA-48, were incubated with 1 mL of serially diluted CCS-$N^+(CH_3)_3$, whose final concentrations were set to 0, 0.08, 0.16, 0.32, 0.64, 0.125, 2.5, 5, and 10 μM in pH 7.4 PBS at 37 °C. The A_{591} values were determined every 30 s, and the initial rates (ν) were determined by the Michaelis–Menten equation

$$\nu = \frac{V_{max}\,[S]}{K_m + [S]}$$

where V_{max} is the maximal reaction rate at which the carbapenemase is sufficient to hydrolyze the substrate CCS-$N^+(CH_3)_3$ and $[S]$ values are the substrate concentration. Based on the Michaelis–Menten equation, five kinetic curves were obtained. To accurately determine the K_m values, five Lineweaver–Burk diagrams were drawn by using the double reciprocal method, where their K_m value was determined according to the y-axis intercept. Finally, the k_{cat} and k_{cat}/K_m values were calculated based on the V_{max} and enzyme concentrations ($k_{cat} = V_{max}/0.2$). Three replicates of parallel samples were tested to offer the standard deviations.

Visual Detection of Clinical Isolates

We screened seven strains of carbapenem-resistant and four strains of non-carbapenem-resistant clinical isolates to evaluate the performance of CCS-$N^+(CH_3)_3$. The 11 strains were cultured in 20 mL of LB medium at 37 °C until the optical density at 600 nm (OD_{600}) reached 0.8–0.9. 100 μL of 0.5% Triton X-100 was added to 1 mL of bacterial solutions and incubated for 10 min, which was quickly frozen in liquid nitrogen and treated ultrasonically for 2 min. 1 μL of each sonicated bacteria lysate was added to 50 μL of CCS-$N^+(CH_3)_3$ solution (10 μM) in PBS (pH = 7.4) and incubated at 37 °C for 5 min. To further study the sensitivity of the probe, the sonicated bacterial lysates were serially diluted in 96-well plates at final concentrations of 0, 3×10^4, 1×10^5, 3×10^5, 1×10^6, 3×10^6, 1×10^7, and 3×10^7 CFU/mL. For the sake of comparison, the Carba NP test was carried out. The Carba NP test solutions A and B were newly prepared according to the CLSI scheme, in which solution A contains 10 mM zinc sulfate and phenol red at pH = 7.8; solution B is the mixture of solution A and 3 mg/mL imipenem. 1 μL of each sonicated bacteria lysate was serially diluted in 96-well plates with final concentrations of 0, 3×10^5, 1×10^6, 3×10^6, 1×10^7, 3×10^7, 1×10^8, and 3×10^8 CFU/mL, followed by incubation with 50 μL of solution A and solution B. The color changes were recorded by photographing at 15 min and 2 h.

Rapid POC Detection of Clinical Sputum Samples

The study was approved by the Ethics Committee of Tianjin First Center Hospital (no. 21977053). Written informed consent was obtained for all participants. The sputum samples were collected from 80 patients with sepsis, which were detected by the CCS-$N^+(CH_3)_3$-based paper chip. 100 μL of 0.5% Triton X-100 was added to 1 mL of patient sputum for 10 min. The mixtures were vortexed for 30 s. The resulting sputum samples (20 μL) were dropped onto the holes of a test paper and kept for 5 min to check the color response. We took pictures of the test paper with a smartphone under the shadowless lamp. The pictures were then dealt with a color recognizer software to convert the colors to the Lab color model, finally yielding the quantifiable a^* values. The a^* channel was selected because green is the complementary color of red, the reaction's endpoint color (green–red, −128 to 127). At the same time, the Carba NP test was carried out for comparison. The Carba NP test solutions A and B were newly prepared according to the CLSI scheme. The same panel of sputum samples (1 μL) was incubated with 50 μL of Carba NP solution A and solution B, separately. The color response was recorded with a smartphone at 2 h.

https://doi.org/10.1021/jacsau.2c00607
JACS Au 2023, 3, 227–238

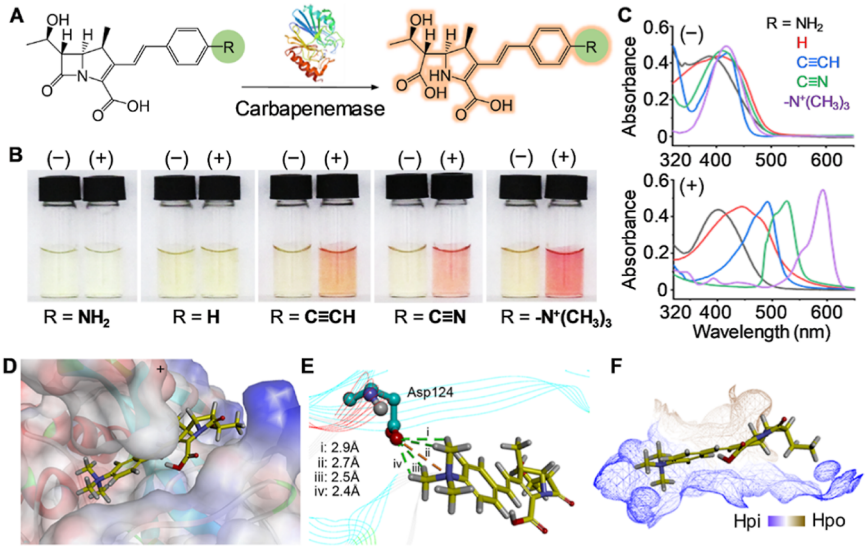

Figure 1. Rational design of CCS for visual detection of carbapenemases. (A) Schematic illustration of carbapenemase-catalyzed cleavage of the β-lactam ring of CCS. (B) Solutions of CCS (10 μM) bearing various substituents were added with PBS alone (−) and NDM-1 (3 nM) (+), respectively. NDM-1 represents one of the most common carbapenemases. (C) UV−vis spectra of solutions in (B). (D) Docking poses of CCS-$N^+(CH_3)_3$ in NDM-1 active site mapped by electrostatic surface potentials. (E) Hydrogen bonding (green dotted line) and electrostatic interactions (orange dotted line) of NDM-1 with CCS-$N^+(CH_3)_3$. The protein structure is simplified with lines. (F) Hydrophobic interactions between CCS-$N^+(CH_3)_3$ and the active region of NDM-1 mapped by Hpo and Hpi, that is, hydrophobicity and hydrophilicity, respectively.

Modified Carbapenem Inactivation Method

The 80 sputum samples were cultured on LB media overnight to produce pure colonies, which were scratched by an inoculated loop. The colony-carried inoculated loop was washed in 2 mL of Tryptic soy broth (TSB), which was then cultured overnight. 1 μL of the cultured colonies was added into another 2 mL of TSB, followed by mixing for 10−15 s to produce bacterial suspensions. A piece of sterile paper containing 10 μg of meropenem was immersed into the bacterial suspension and incubated at 37 °C for 4 h. In parallel, a suspension of *E. coli* (ATCC 25922) was prepared with normal saline at 0.5 Maxwell turbidity. The freshly prepared *E. coli* suspension was sprayed on Mueller−Hinton agar solid media within 15 min and dried for 10 min. After that, the sample-treated sterile papers were attached to *E. coli*-covered culture media and incubated at 37 °C for 24 h. Finally, the diameter of inhibition zones was measured to assess the antibiotic level.

Carbapenem-Resistant Gene Profiling with RT-PCR

We first searched the standard sequences of bla_{NDM}, bla_{IMP}, bla_{KPC}, bla_{VIM}, and bla_{OXA-48} from GenBank (https://www.ncbi.nlm.nih.gov/) and designed the primers by Primer 6.0 software. The sequences of the designed primers are shown in Table S3. Then, the primers were synthesized by Sangon Biotech, a commercial supplier. The bacterial DNA was extracted by the boiling template method. The sputum samples from the 80 sepsis patients were smeared on LB solid medium and cultured for 24 h at 37 °C. Two inoculate ring bacterial lawns were scraped and added to 150 μL PBS (pH = 7.8), evenly mixed and boiled for 10 min at 100 °C, and then centrifuged at 12 000 r/min for another 10 min. The supernatants containing bacterial DNA were collected and stored at −20 °C. Bacterial DNA and primers were mixed with a SGExcel FastSYBR mixture following the SGExcel FastSYBR qPCR Mixture instructions (Table S4). RT-PCR parameters were set according to Table S5 and performed by the LightCycler 96 instrument (Roche, Switzerland).

RESULTS AND DISCUSSION

Rational Design and Synthesis of CCSs

Three key building blocks, including the carbapenem core structure, a conjugated benzene derivative, and a terminated para-substituent, were modularly designed to constitute the CCS structure (Figure 1A). First, the carbapenem core acts as the recognition group of CCSs offering high specificity toward carbapenemase.[16] Second, a benzene derivative is conjugated to the 3-position of the carbapenem core via a double bond, producing a chromogenic compound whose absorption spectrum appears in the 350 to 500 nm region. Lastly, the chromogenic properties of CCSs and their corresponding products can be well modulated by further conjugated para-substituents with different electronegativities. The electronegativity of the substituent is highly related to the red shift of UV−vis absorption and thus the shifting of color.[28] We assumed that CCSs show yellow color in aqueous solutions. When the β-lactam ring of CCSs is cleaved by carbapenemases, the amide nitrogen is transformed into a secondary amine, leading to the resonance change in the extended conjugated system.[29] Consequently, the absorption bands undergo a red shift in the visible region, accompanied by a striking color change from yellow to red.

To confirm the above hypothesis, we synthesized five CCS-bearing substituents with different electronegativities, including three electron-withdrawing groups [$-N^+(CH_3)_3$, $-C{\equiv}N$, and $-C{\equiv}CH$] and one electron-donating group ($-NH_2$); no substituent was set as a control. As shown in Scheme S1 (Supporting Information), CCSs were synthesized from the commercially available meropenem intermediate 1, whose carboxyl group had already been protected by 4-nitrobenzoic acid (PNB). The hydroxyl group in 1 was first protected by *tert*-butyldimethylsilyl chloride (TBS) to afford compound 2. After a rhodium-catalyzed ring closure, the ensuing ketone was transformed into hydroxyl, which was subsequently protected by trifluoromethanesulfonyl (Tf) to yield compound 3. By means of a Stille coupling reaction, the Tf-protected hydroxyl (−OTf) was replaced by a vinyl group, producing the key intermediate 4. Removal of the protecting group TBS with $NH_4{\cdot}HF_2$ provided compound 5, followed by removing the other protecting group PNB through Pt/C catalysis to afford compound 6. Ultimately, compound 6 was conjugated with

https://doi.org/10.1021/jacsau.2c00607
JACS Au 2023, 3, 227−238

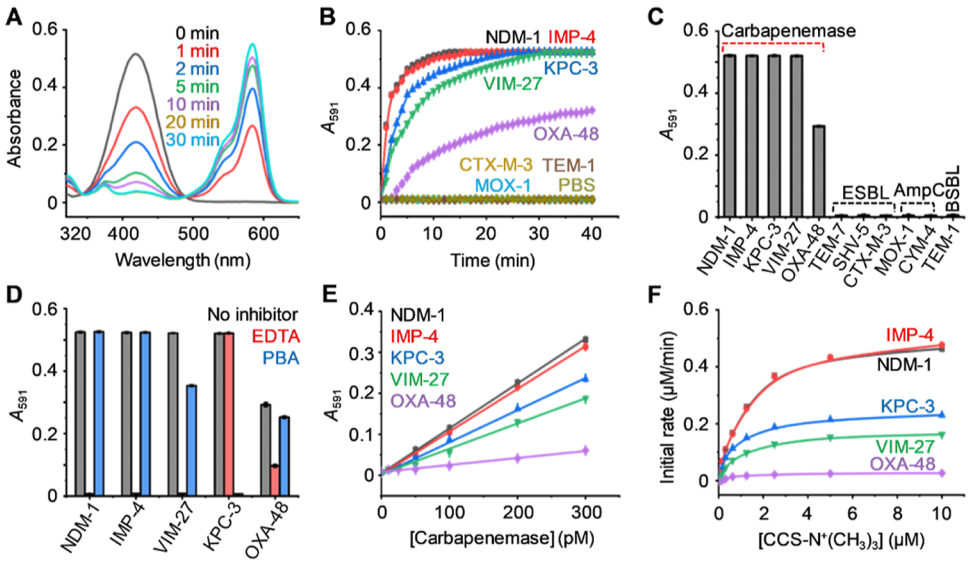

Figure 2. Analytical features of CCS-$N^+(CH_3)_3$ toward carbapenemases. (A) Spectral change of CCS-$N^+(CH_3)_3$ (10 μM in PBS, pH 7.4) over time after incubation with NDM-1 (3 nM). (B) Absorbance change at 591 nm (A_{591}) of CCS-$N^+(CH_3)_3$ (10 μM in PBS, pH 7.4) over time toward 3 nM of carbapenemases (NDM-1, KPC-3, IMP-4, VIM-27, and OXA-48) and 30 nM of non-carbapenemases (CTX-M-3, MOX-1, and TEM-1). (C) A_{591} of CCS-$N^+(CH_3)_3$ in (B) after incubation of selected β-lactamases for 30 min. (D) A_{591} of CCS-$N^+(CH_3)_3$ (10 μM in PBS, pH 7.4) after incubation with selected carbapenemases and corresponding inhibitors for 30 min. (E) A_{591} of CCS-$N^+(CH_3)_3$ (10 μM in PBS, pH 7.4) after incubation with various concentrations of selected carbapenemases for 30 min. (F) Michaelis–Menten kinetic plots of selected carbapenemases toward CCS-$N^+(CH_3)_3$. The error bars represent the standard deviations of three replicates.

bromobenzenes bearing various substituents via the Heck coupling reaction under alkaline conditions, affording CCSs with different yields: CCS-H (54%), CCS-NH_2 (62%), CCS-C≡CH (47%), CCS-C≡N (45%), and CCS-$N^+(CH_3)_3$ (30%). These products and related intermediates were characterized by NMR and mass spectroscopy (MS), as shown in Figures S1–S33, Supporting Information.

Experimental Validation of Carbapenemase-Catalyzed Hydrolysis of CCSs

According to the amino acid homologies, carbapenemases are classified into A, B, and D β-lactamases.[30] To evaluate the coverage of CCS, we prepared five kinds of carbapenemases, namely, KPC-3, NDM-1, VIM-27, IMP-4, and OXA-48, whose corresponding families (KPC, NDM, VIM, IMP, and OXA-48-like) account for >99% of carbapenemase-producing isolates.[31] KPC-3 and OXA-48 represent the most clinically prevalent carbapenemases in classes A and D, respectively, both of which belong to serine hydrolases; NDM-1, VIM-27, and IMP-4 are the typical carbapenemases in class B, a kind of Zn-dependent metallo-β-lactamases. At the same time, six kinds of other β-lactamases were prepared as negative controls to examine the selectivity of CCS, including three ESBLs (SHV-5, TEM-7, and CTX-M-3),[32,33] two AmpC β-lactamases (MOX-1 and CMY-4),[34] and one BSBL (TEM-1).[35] These β-lactamases were synthesized with genetic engineering techniques according to their corresponding gene sequences. The yielded β-lactamases were purified by HisTrap Ni columns and characterized by SDS-PAGE (Figures S34–S44).

With CCSs and carbapenemases in hand, we attempted to investigate their interactions. Upon incubating various CCSs (10 μM) with the typical carbapenemase–NDM-1 (3 nM) in phosphate-buffered saline (PBS, pH = 7.4) at 37 °C, the solutions of CCS-$N^+(CH_3)_3$, CCS-C≡N, and CCS-C≡CH underwent a color change immediately from pale yellow to red (Figure 1B). The red degree was positively correlated with the electron-withdrawing ability of the substituents: $-N^+(CH_3)_3$ > −C≡N > −C≡CH. By contrast, the solutions of CCS-NH_2 and CCS-H have no noticeable change, most likely owing to the poor electronegativity of $-NH_2$ and −H. As a control, all the five CCS solutions remained pale yellow in the presence of PBS alone, demonstrating their excellent chemical stability. The naked eye results were confirmed by UV–vis spectra. The maximal absorption bands (λ_{max}) of all CCSs appear at around 400 nm (Figure 1C, top); after the rupture of the β-lactam rings, the λ_{max} red-shifts in the visible regions, where the wavelength coincides with the electron-withdrawing capability of the substituents (Figure 1C, bottom). These experimental results agree well with the hypothesis described above.

To validate whether CCSs were efficiently cleaved by NDM-1, the five CCSs and their hydrolysates were purified and analyzed with LC–MS. As shown in Figures S45–S49, the LC retention time of all the hydrolysates became shorter than that of the corresponding CCSs, and no other LC peaks were observed. These results demonstrate that the β-lactam rings in all CCSs were entirely cleaved, and no intermediates were produced during the hydrolysis. These compounds were characterized by MS. Compared with CCSs, the corresponding hydrolysates showed an expected mass increase of 18 amu for all the major peaks, indicating the successful hydrolysis of the amide in the β-lactam ring into −COOH and a secondary amine. The purified CCS hydrolysates were further analyzed by ^{1}H NMR and UV–vis spectroscopy. The ^{1}H NMR spectra show that the peaks of the hydrogens neighboring the β-lactam ring are obviously different between CCSs and their corresponding hydrolysates. In particular, a single peak at around 6.5 ppm was found in all the hydrolysates, which is assigned to the secondary amine transformed from the 5-amide nitrogen, directly demonstrating the rupture of the β-lactam ring. The UV–vis spectra (Figure S50) of the purified CCS hydrolysates were found the same as those without purification (as shown in Figure 1C, bottom), eliminating the influence of

https://doi.org/10.1021/jacsau.2c00607
JACS Au 2023, 3, 227–238

the co-existing species on the spectra. Because the only structural difference between the five hydrolysates is the substituents, the red shift of wavelength can only be ascribed to their different electron-withdrawing capability. These results proved that all the five as-prepared CCSs possess high reactivity with NDM-1. Therefore, the negligible color change of CCS-NH_2 and CCS-H before and after structure rupture is mostly ascribed to their poor chromogenicity other than reactivity.

Molecular Simulations

After experimental validation, we attempted to reveal the interactions between CCSs and NDM-1 using molecular simulations. The optimal docking poses of NDM-1 with the five CCSs were described using High Ambiguity Driven protein−protein DOCKing (HADDOCK),[36] which shows that the active cavities of NDM-1 are flexible to accommodate all the CCSs (Figures 1D and S51). The intermolecular interactions between CCSs and NDM-1 include electrostatic forces, van der Waals forces, and hydrophobic interactions. Ionic bonding and hydrogen bonding represent two typical electrostatic forces to drive the complexing between NMD-1 and CCSs. The simulation results show that CCS-H, CCS-C≡N, CCS-C≡CH, and CCS-$N^+(CH_3)_3$ possess different numbers of hydrogen bonds toward NMD-1. Meanwhile, the positively charged -$N^+(CH_3)_3$ provides a distinct ionic bonding toward the negatively charged Asp124 in the binding site of NDM-1 (Figure 1E), resulting in high affinity. In addition, hydrophobic interactions also contribute to the molecular binding in the hydrophobic regions of NDM-1 (Figure 1F).

We further calculated the docking parameters of these complexes to evaluate their overall binding affinities (ΔG) (Table S1). PRODIGY was utilized to measure the ΔG values of NMD-1 toward the five CCSs based on the optimal docking complexes.[37,38] The ΔG values of CCS-NH_2 and CCS-H toward NMD-1 were determined to be −7.3 and −8.1 kcal/mol, respectively. By contrast, the assemblies of NMD-1 with CCS-C≡CH (−9.4 kcal/mol) and CCS-C≡N (−8.8 kcal/mol) show stronger ΔG values because of their higher HADDOCK scores and much stronger electrostatic interactions. As anticipated, the complex of NDM-1 with CCS-$N^+(CH_3)_3$ possesses the highest HADDOCK score (−67.1 ± 3.0) and the strongest affinity of −9.9 kcal/mol, which stems mainly from the solid electrostatic interactions caused by the electro-positively charged -$N^+(CH_3)_3$. To this end, -$N^+(CH_3)_3$ acts as not only an electron-withdrawing moiety but also a high-affinity binding site with carbapenemases, contributing collectively to the high sensitivity of CCS-$N^+(CH_3)_3$.

Analytical Features of CCS-$N^+(CH_3)_3$

Because CCS-$N^+(CH_3)_3$ offers the highest electron-withdrawing ability and binding affinity with NDM-1, we conducted the following studies with CCS-$N^+(CH_3)_3$. As indicated by UV−vis spectra (Figure 2A), CCS-$N^+(CH_3)_3$ (10 μM in PBS, pH 7.4) alone shows a single absorption band at 417 nm. With the addition of NDM-1 (3 nM), the pale-yellow color turned red within several seconds, leading to a gradual decrease of the absorbance at 417 nm, along with the emergence of a new absorption band at 591 nm whose intensity is dependent on the incubation time. It is extremely impressive that the two bands at 417 and 591 nm can be completely resolved, without any spectral overlap. Moreover, the absorbance of CCS-$N^+(CH_3)_3$ at 591 nm is extremely low (∼0.004). After adding NDM-1, over 120-fold enhancement of absorbance was achieved in 5 min. Therefore, the change of absorbance at 591 nm (A_{591}) could be employed to report the presence of carbapenemases sensitively.

We then evaluated the selectivity of CCS-$N^+(CH_3)_3$ toward the as-prepared carbapenemases (NDM-1, KPC-3, IMP-4, VIM-27, and OXA-48) over other non-carbapenemase β-lactamases including CTX-M-3, MOX-1, and TEM-1 that belong to ESBLs, AmpC, and BSBL, respectively. Upon incubating CCS-$N^+(CH_3)_3$ (10 μM) with the five carbapenemases (3 nM), all the solutions became red immediately, along with a dramatic enhancement of A_{591}. As depicted in Figure 2B, the A_{591} values for NDM-1 and IMP-4 reached the maximum within 10 min and remained stable with further incubation time, while those for KPC-3, VIM-27, and OXA-48 arriving at their plateaus required a longer time, indicating lower hydrolysis capability. By contrast, the three non-carbapenemase β-lactamase-treated CCS-$N^+(CH_3)_3$ solutions showed negligible color change even the enzyme concentrations were increased to 30 nM, 10-fold higher than that of the carbapenemases. Accordingly, their A_{591} values approached zero during the whole detection period. By collecting the absorbance at 30 min, the A_{591} values of the CCS-$N^+(CH_3)_3$ solutions added with NDM-1, KPC-3, IMP-4, and VIM-27 were calculated to be ∼0.52, >100-fold higher than that of the CCS-$N^+(CH_3)_3$ solutions alone (Figure 2C), while that added with OXA-48 was enhanced to be ∼0.3. It has been reported that OXA-48 possesses much lower hydrolytic activity than the other carbapenemases,[16−19,39] making it difficult to detect with existing chemical probes. The ability to detect OXA-48 by the naked eye demonstrates the high sensitivity of CCS-$N^+(CH_3)_3$. No surprisingly, the A_{591} values for the cases of CTX-M-3, MOX-1, and TEM-1 remained to be approximately zero. These results confirm that CCS-$N^+(CH_3)_3$ possesses excellent performance to detect various carbapenemases.

To validate the selectivity of CCS-$N^+(CH_3)_3$ toward carbapenemases, we employed inhibition assays to investigate the effects of PBA (a KPC-specific inhibitor) and EDTA (a metallo-β-lactamase inhibitor) on the carbapenemase-induced hydrolysis of CCS-$N^+(CH_3)_3$.[40,41] The results show that PBA could significantly reduce the enzymatic activity of KPC-3. In contrast, the activity of NDM-1, IMP-4, VIM-27, and OXA-48 was minimally affected (Figure 2D). On the other hand, the presence of EDTA could markedly blunt the enzymatic activities of NDM-1, IMP-4, and VIM-27. However, the activity of KPC-3 was negligibly impacted. We note that the addition of EDTA could slightly impair the activity of OXA-48, which is likely due to the enzymatic deactivation caused by the increased concentration of ions.[42]

Sensitivity is another important parameter of a probe particularly applied in clinical practice. Through incubation of CCS-$N^+(CH_3)_3$ (10 μM) with various concentrations (0, 10, 25, 50, 100, 200, and 300 pM) of carbapenemases in a 96-well microplate for 30 min, the absorbance at 591 nm (A_{591}) was recorded with a microplate reader. By plotting the A_{591} values versus the concentrations of carbapenemases, five calibration curves were created at $3S/k$ (where S is the standard deviation of the blank sample and k is the slope of the calibration curve), by which the limits of detection (LODs) for NDM-1, IMP-4, KPC-3, VIM-27, and OXA-48 were calculated to be 3.1, 3.3, 4.4, 5.6, and 20.3 pM, respectively (Figure 2E), with a dynamic linear range from 10 to 300 pM. Though CCS-C≡CH and CCS-C≡N show a similar tendency toward the same panel of carbapenemases, their LODs are a little higher

https://doi.org/10.1021/jacsau.2c00607
JACS Au 2023, 3, 227−238

than those obtained by CCS-$N^+(CH_3)_3$ (Figure S52). To the best of our knowledge, our CCSs are the first colorimetric probes that could detect carbapenemases (encompassing OXA-48 in particular) at picomolar levels without resorting to signal amplification strategies or/and complex readout equipment.

To better understand the enzymatic hydrolysis of carbapenemases toward CCS-$N^+(CH_3)_3$, we measured the Michaelis−Menten kinetic parameters, including the Michaelis (K_m) and catalytic constant (K_{cat}) by creating Lineweaver−Burk plots. The results show that CCS-$N^+(CH_3)_3$ could be rapidly hydrolyzed by the carbapenemases (Figure 2F). The kinetic efficiencies (K_{cat}/K_m) of NDM-1, IMP-4, KPC-3, and VIM-27 were estimated to be on the order of 10^7 M^{-1} s^{-1}, while that of OXA-48 was determined to be 1.94×10^6 M^{-1} s^{-1} (Table 1). The K_{cat}/K_m values of the carbapenemases

Table 1. Michaelis−Menten Kinetics for Carbapenemases[a]

carbapenemase	k_{cat} (s^{-1})	K_m (μM)	k_{cat}/K_m (M^{-1} s^{-1})
NDM-1	26.29 ± 0.98	1.21 ± 0.13	2.17×10^7
IMP-4	27.65 ± 1.07	1.37 ± 0.15	2.01×10^7
KPC-3	12.66 ± 0.22	0.77 ± 0.04	1.64×10^7
VIM-27	9.16 ± 0.19	1.01 ± 0.06	9.07×10^6
OXA-48	1.32 ± 0.07	0.68 ± 0.09	1.94×10^6

[a]The errors represent the standard deviations of three parallel samples.

toward CCS-$N^+(CH_3)_3$ are comparable to those toward imipenem and meropenem but higher than those toward the carbapenem-based fluorogenic probes by 1−2 orders of magnitude,[15,16] confirming the high reactivity of CCS-$N^+(CH_3)_3$.

Further, the molar extinction coefficient (a parameter to assess the sensitivity of a dye) of CCS-$N^+(CH_3)_3$ was determined to be 47 061 L mol^{-1} cm^{-1} via the Lambert−Beer law (Figure S53). Besides, the chemical stability of CCS-$N^+(CH_3)_3$ was investigated by testing its background hydrolysis via a first-order kinetic curve (Figure S54), based on which the pseudo-first-order rate constant and half-life for the spontaneous hydrolysis reaction (PBS, pH 7.4) of CCS-$N^+(CH_3)_3$ at room temperature were estimated to be 4.1×10^{-6} s^{-1} and 47 h, respectively, outperforming the similar carbapenemase probe.[19]

High-Sensitivity Detection of Clinical CPB Isolates by the Naked Eye

Having demonstrated that CCS-$N^+(CH_3)_3$ can selectively and sensitively detect carbapenemases, we investigated its capability to detect the clinically frequent CPB isolates including *E. coli* (*E. coli*), *Pseudomonas aeruginosa* (*P. aeruginosa*), and *Klebsiella pneumoniae* (*K. pneumoniae*). The clinical CPB isolates were quickly treated with freezing and sonication to prompt the release of carbapenemases from bacteria. In addition to *E. coli* encoded with NDM-1 (strain 1) whose enzymatic activity has been well tested by CCS-$N^+(CH_3)_3$, we extended our investigation to another *E. coli* that produces NDM-5 (a homologue of NDM-1) (strain 2) to confirm the pan-carbapenemase coverage of this substrate (Figure 3A). Moreover, we demonstrated that the presence of non-carbapenemase ESBL (e.g., CTX-M-14) in the NDM-1-encoded *E. coli* (strain 3) would not interfere obviously with the enzymatic activity of NDM-1. As expected, OXA-48-encoded *E. coli* (strain 4) can also be well detected by CCS-$N^+(CH_3)_3$. We further demonstrated that CCS-$N^+(CH_3)_3$ possessed the unique ability to detect *P. aeruginosa* and *K. pneumoniae* expressed with KPC-2 or IMP-2 (strains 5−7). By contrast, CCS-$N^+(CH_3)_3$ did not respond to the non-carbapenemase-producing isolates (strains 8−11) under the same measurement conditions. Note that the expressions of

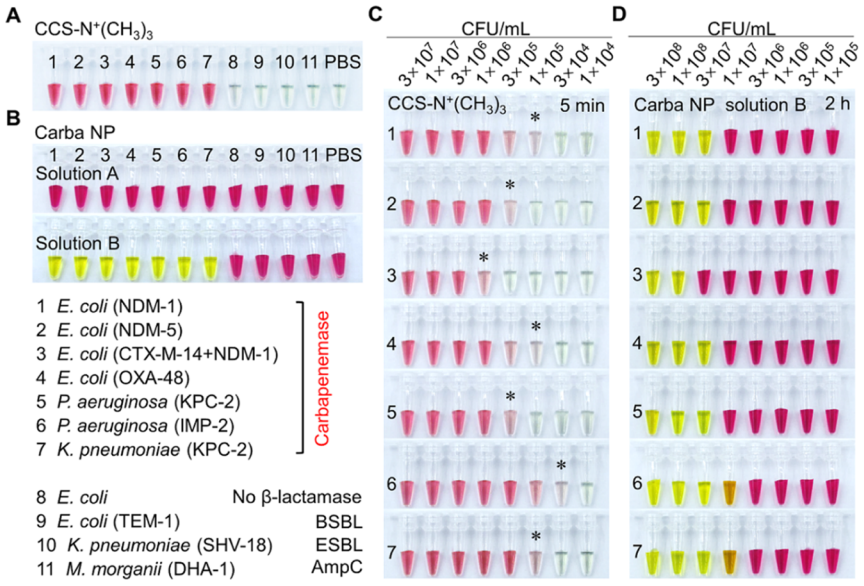

Figure 3. Naked eye detection of the sonicated lysates of clinical CPB isolates. Chromogenic response of (A) CCS-$N^+(CH_3)_3$ (10 μM) and (B) Carba NP solution A and solution B to the sonicated lysates of diverse clinical isolates including seven carbapenemase-encoded strains and three non-carbapenemase-encoded strains. E. coli without β-lactamase expression was set as a control. Chromogenic response of (C) CCS-$N^+(CH_3)_3$ (10 μM) and (D) Carba NP solution B to the seven clinical CPB lysates at varying concentrations. The images for CCS-$N^+(CH_3)_3$ and Carba NP were taken after incubation for 5 min and 2 h, respectively. The asterisks indicate the lowest detectable concentrations of the clinical CPB isolates by the naked eye.

https://doi.org/10.1021/jacsau.2c00607
JACS Au 2023, 3, 227−238

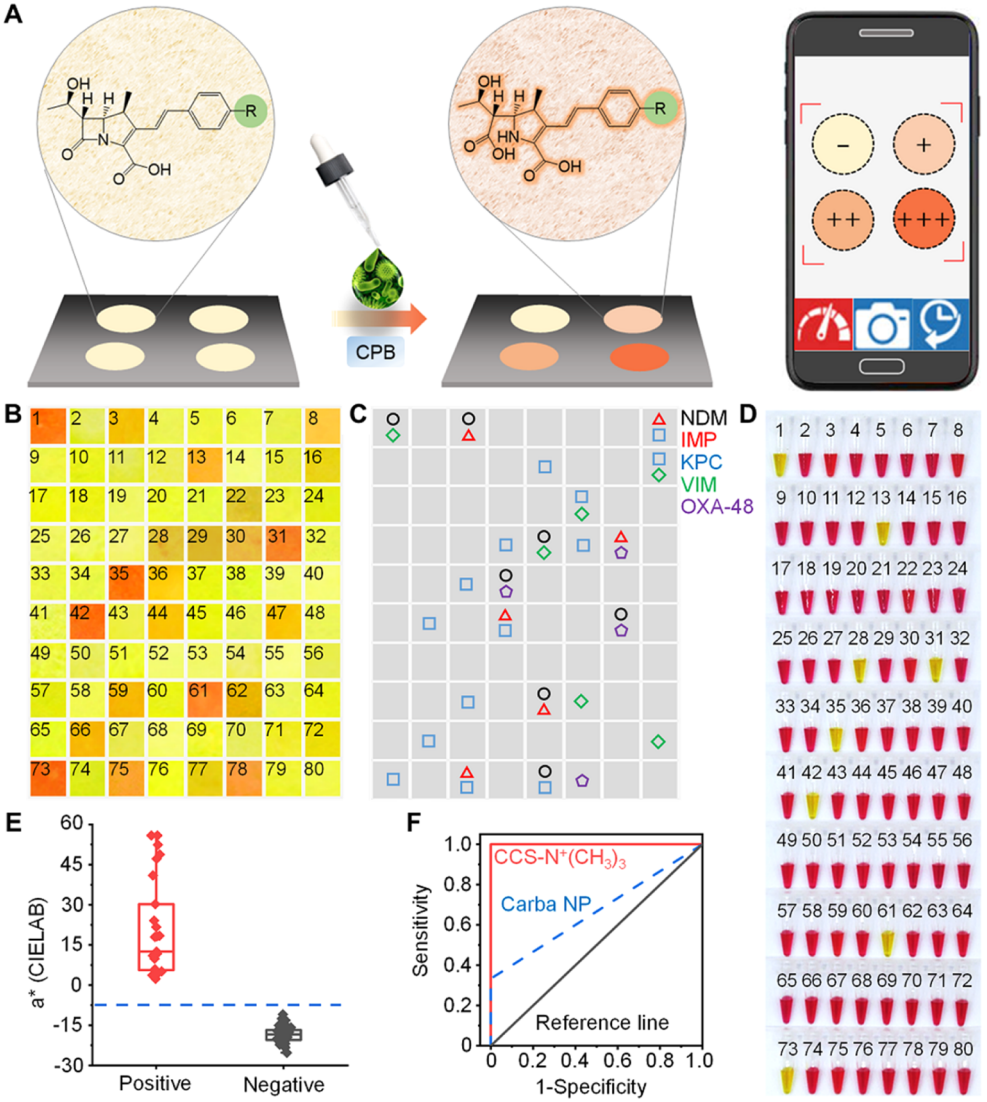

Figure 4. Detection of CPB in the clinical sputum samples collected from lung-infected patients. (A) Schematic of visual detection of CPB on a paper chip, where the color changes can be quantitatively identified by a smartphone installed with a color recognizer software. The *a** values reflecting colors from green to red were recorded in the CIELAB (Lab) color model. (B) 80 culture-free sputum samples detected by the CCS-$N^+(CH_3)_3$-loading paper chips. (C) Carbapenem-resistant genes in the same culture-free 80 samples analyzed by RT-PCR. Each square corresponds to the paper block in (B). (D) Carba NP test (solution B) toward the same 80 cultured samples at 2 h (the results of solution A are provided in Figure S58). (E) Statistics of the *a** values for the naked eye results in (B). (F) ROC curves of the CCS-$N^+(CH_3)_3$-based POC method and the Carba NP test.

relevant β-lactamase-encoding genes in these isolates had been well characterized by PCR in the clinic.

The detection results for the sonicated bacteria lysates were compared with Carba NP test, a commonly used approach for visual detection of carbapenemases as well as CPB. According to the CLSI protocol, Carba NP test relies on two solutions: solution A and solution B. Solution A consists of sodium hydroxide, phenol red, and zinc sulfate; solution B includes solution A and imipenem. When the above-mentioned isolates were incubated with solution B, the β-lactam ring of imipenem was hydrolyzed by the CPB (strains 1−7) to produce a carboxylic acid. As a consequence, the pH of the solution was lowered to cause a color change of phenol red from red to yellow in 2 h (Figure 3B). At the same time, the non-carbapenemase-expressed isolates (strains 8−11) could not change the color of solution B. Solution A was used as quality control that did not show any positive color change for all the 11 strains. These results confirm the accuracy of CCS-$N^+(CH_3)_3$ for rapid detection of clinical CPB lysates by the naked eye.

To determine the sensitivity of our new probe, serial dilutions of the above clinical CPB lysates (strains 1−7, 1 μL) were incubated with CCS-$N^+(CH_3)_3$ (10 μM, 50 μL). With the increase of CPB concentrations, a gradual color change from pale yellow to red occurred in a few minutes. The lowest detectable concentrations varied across 10^4 to 10^6 CFU/mL levels among different strains (Figure 3C). The lowest detectable concentration for *P. aeruginosa* (IMP-2, strain 6) was determined to be 3×10^4 CFU/mL (1500 CFU), while those for *E. coli* (NDM-1, strain 1), *E. coli* (OXA-48, strain 4), and *K. pneumoniae* (KPC-2, strain 7) were determined to be 1×10^5 CFU/mL (5000 CFU). With respect to *E. coli* (NDM-5, strain 2) and *P. aeruginosa* (KPC-2, strain 5), the lowest detectable concentrations were determined to be 3×10^5

https://doi.org/10.1021/jacsau.2c00607
JACS Au 2023, 3, 227−238

CFU/mL (15 000 CFU). *E. coli* (CTX-M-14 + NDM-1, strain 3) showed the lowest detectable concentration of 1×10^6 CFU/mL (50 000 CFU). As indicated by the asterisks, the color change at the lowest detectable concentrations of carbapenemases can be notably discriminated by the naked eye.

In parallel, the same panel of sonicated bacteria lysates was detected by the Carba NP test. Strains 1, 2, 4, 6, and 7 were positively detected within 5 min, with ~10^8 CFU/mL levels of detection limits, while strains 3 and 5 were unresponsive to the Carba NP test during the same period (Figure S55). With prolonged incubation time to 2 h, the detection limits for all the strains were improved to be ~10^7 CFU/mL levels (Figure 3D), still higher than that of the CCS-$N^+(CH_3)_3$-based assay by 2−3 orders of magnitude. Because the concentrations of CPB isolates in unprocessed clinical sputum samples are in the range of 3.5×10^6 to 6.1×10^7 CFU/mL (Figure S56), the Carba NP test can only detect the samples whose CPB concentrations are higher than 1.0×10^7 CFU/mL levels. By contrast, the ultrahigh sensitivity of CCS-$N^+(CH_3)_3$ makes it fully competent for the direct detection of CPB in real clinical samples.

Direct Detection of CPB in the Sputum of Lung-Infected Patients with Sepsis

Sepsis is a systemic inflammatory response syndrome caused by infections complicated with multiple organ failure, which leads to high morbidity and mortality.[43] It is estimated that more than 30 million cases of sepsis are diagnosed every year worldwide, resulting in about 6 million deaths annually.[44] Lung infections are the main cause of sepsis, especially in intensive care units, and patients who suffer from sepsis with lung infections have a higher mortality rate than those without lung infections.[45,46] CPB has become the most dangerous pathogen causing lung infections in sepsis patients. Therefore, it is highly desirable to develop rapid POC assays for CPB in the clinic.

To better conduct the POC testing, we transferred the CPB detection from aqueous solutions to a paper chip that has been widely developed for a variety of applications.[47,48] CCS-$N^+(CH_3)_3$ was loaded in a paper chip for visual detection, where the results can be quantitatively analyzed via a smartphone (Figures 4A and S57). In parallel, we collected 80 sputum samples from patients with sepsis, most of whom were infected by antibiotic-resistant pathogens (Table S2). 20 μL of each sonicated sputum sample was spotted onto the CCS-$N^+(CH_3)_3$-loaded paper chip, where the reaction proceeded at room temperature. 24 out of 80 cases were visualized with color changes from pale yellow to red at a sample-to-result time of less than 15 min (Figure 4B). The change in color intensity varied among the 24 positive samples. To validate these results, RT-PCR was employed to detect the genes that encode NDM, IMP, KPC, VIM, and OXA-48 throughout the 80 sputum samples (Tables S3−S5). It is observed that only one or two kinds of carbapenemase genes with different expression signatures were positively detected in the 24 positive samples with color change (Figure 4C), while no carbapenemase genes can be detected in the rest 56 samples, fully supporting the visual results. By contrast, only eight samples (no. 1, 13, 28, 31, 35, 42, 61, and 73) were positively detected by the Carba NP test (Figures 4D and S58) even within 2 h, due to its poor sensitivity.

The visual results can be quantitatively analyzed by converting the colors into the a^* values of CIELAB (Lab) with a smartphone installed with a color recognizer software.[49] Lab color model includes all the colors that can be seen by the human eye theoretically. It expresses color as three values: L^* for the lightness from black to white, a^* from green to red, and b^* from blue to yellow. Obviously, the a^* values are more suitable than the other two values for quantifying the color changes of the paper chips. The a^* values were directly reported by a smartphone installed with a color recognizer software (Figure S59), without resorting to professional graphics software like Photoshop. With the a^* values of all the 80 clinical samples in hand, a clinical threshold (as indicated by a horizontal dotted line) was defined to differentiate the positive and negative samples. As shown in Figure 4E, the 24 carbapenemase-positive cases are above the threshold, while those of the rest 56 cases are below the threshold.

Receiver operating characteristic curves were developed to evaluate the clinical sensitivity and specificity of our method, which were compared to that of the Carba NP test.[50] The RT-PCR results were set as the reference. Both the clinical sensitivity and specificity of our method were found to be 100% (Figure 4F). Meanwhile, the clinical sensitivity for the Carba NP test was determined to be only 33.3%, along with 100% clinical specificity. The results further confirmed that CCS-$N^+(CH_3)_3$ is advantageous over the Carba NP test in sensitivity and speed, and over RT-PCR in simplicity, speed, and cost.

Finally, modified carbapenem inactivation method (mCIM), a phenotypic assay currently recommended by Performance Standards for Antimicrobial Susceptibility Testing 2018,[51] was employed to validate the detection results of the CCS-$N^+(CH_3)_3$-based POC platform. The mCIM results show that the sputum-treated meropenem papers inhibited the growth of *E. coli* at varying degrees (Figure S60). The bacteriostatic zones of the 24 CPB-positive samples were less than 19 mm in diameter (a typical cutoff to differentiate positive and negative mCIM results[52]), while the rest of the 56 CPB-negative samples were above 19 mm (Table S6). These results proved that the bacteria in the 24 samples are indeed carbapenem-resistant, indicating the high accuracy of our new-type chromogenic probes.

CONCLUSIONS

We designed and synthesized an ultrasensitive and selective carbapenemase probe based on CCS for rapid and direct detection of CPB in clinical sputum by the naked eye. In contrast to the previously reported carbapenemase-specific molecular probes, CCS is simple in structure but shows many superior analytical features (the details are shown in Table S7). We discovered that the conjugated positively charged substituent [such as $-N^+(CH_3)_3$] in CCS can not only boost the red shift of the absorption band but also enhance the molecular interactions toward carbapenemases, thus dramatically improving the sensitivity of the chromogenic probe. The yielded CCS-$N^+(CH_3)_3$-based assay matches the clinical sensitivity and specificity offered by sputum culture that needs days to complete.

Compared to clinically available assays (e.g., traditional culturing methods, RT-PCR gene analysis, and Carba NP test) for CPB, the newly developed CCS-$N^+(CH_3)_3$-based chip assay shows several extraordinary analytical features in the context of simplicity, rapidity, accuracy, and cost (Figure 5). First, this chromogenic assay is culture-free, does not require

https://doi.org/10.1021/jacsau.2c00607
JACS Au 2023, 3, 227−238

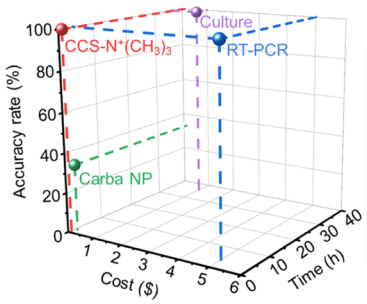

Method	Cost ($)	Time (h)	Accuracy rate (%)
Culture	1	36	100
RT-PCR	5	4	100
Carba NP	0.1	2	33.3
CCS-$N^+(CH_3)_3$	0.1	0.25	100

Figure 5. Analytical performance comparison. Three-dimensional comparison of the CCS-$N^+(CH_3)_3$-based POC chip, Carba NP test, RT-PCR, and culture-based assays in the context of cost, processing time, and accuracy rate.

instrument and complex sample pretreatment, and delivers results in several minutes by the naked eye, much faster than the other techniques. Second, the detection accuracy of CCS-$N^+(CH_3)_3$ for clinical testing is comparable to those of RT-PCR and culturing methods, yet much higher than that of the Carba NP test. Third, each test of the CCS-$N^+(CH_3)_3$-based paper chip only costs ~US$0.1, equal to the Carba NP test but much cheaper than RT-PCR (~US$5) and culturing methods (~US$1). This user-friendly POC assay allowed rapid identification of CPB in the clinical sputum samples from 80 sepsis patients. To the best of our knowledge, CCS-$N^+(CH_3)_3$ is the first chemical probe that is able to detect CPB in real clinical samples with 100% sensitivity and specificity.

The push−pull electronic effect-enhanced molecular design of CCS can be generalized for visual detection of other species of interest simply by changing the recognition moiety. Future work will focus on extending this effective strategy to develop high-sensitivity chromogenic substrates for other β-lactamases such as BSBL, ESBL, and AmpC, which will be combined with CCS-$N^+(CH_3)_3$ on a paper chip for rapid discrimination of antibiotic resistance to aid effective antimicrobial stewardship, especially in resource-poor settings.

■ ASSOCIATED CONTENT

Supporting Information

The Supporting Information is available free of charge at https://pubs.acs.org/doi/10.1021/jacsau.2c00607.

Experimental procedures; sequences of the β-lactamases and SDS-PAGE data; molecular simulation details; first-order kinetic plot; Carba NP test; statistics of the CPB colonies in clinical sputum samples; clinical information for sputum samples; working interface of color recognizer Android software; docking details; RT-PCR reaction system and response procedures; diameter of bacteriostatic probes; ; analytical and spectroscopic data for the new compounds; and copies of UV−vis spectra, HPLC spectra, ^{1}H NMR spectra, ^{13}C NMR spectra, and HRMS data (PDF)

■ AUTHOR INFORMATION

Corresponding Author

Dingbin Liu − *State Key Laboratory of Medicinal Chemical Biology, Research Center for Analytical Sciences, and Tianjin Key Laboratory of Molecular Recognition and Biosensing, Frontiers Science Center for New Organic Matter, College of Chemistry, Nankai University, Tianjin 300071, China;* orcid.org/0000-0003-4153-9822; Email: liudb@nankai.edu.cn

Authors

Wenshuai Li − *State Key Laboratory of Medicinal Chemical Biology, Research Center for Analytical Sciences, and Tianjin Key Laboratory of Molecular Recognition and Biosensing, Frontiers Science Center for New Organic Matter, College of Chemistry, Nankai University, Tianjin 300071, China*

Jingjing Wang − *Department of Intensive Care Unit, Key Laboratory for Critical Care Medicine of the Ministry of Health, Emergency Medicine Research Institute, Tianjin First Center Hospital, School of Medicine, Nankai University, Tianjin 300071, China*

Chen Li − *College of Arts and Sciences, Shanxi Agricultural University, Taigu 030801, China*

Zhiyou Zong − *State Key Laboratory of Medicinal Chemical Biology, Research Center for Analytical Sciences, and Tianjin Key Laboratory of Molecular Recognition and Biosensing, Frontiers Science Center for New Organic Matter, College of Chemistry, Nankai University, Tianjin 300071, China*

Jinzhong Zhao − *College of Arts and Sciences, Shanxi Agricultural University, Taigu 030801, China*

Hongmei Gao − *Department of Intensive Care Unit, Key Laboratory for Critical Care Medicine of the Ministry of Health, Emergency Medicine Research Institute, Tianjin First Center Hospital, School of Medicine, Nankai University, Tianjin 300071, China*

Complete contact information is available at: https://pubs.acs.org/10.1021/jacsau.2c00607

Author Contributions

W.L. and D.L. designed the study. J.W. and H.G. provided clinical samples and related information. W.L. and C.L. performed the experiments. Z.Z. provided molecular simulation results. W.L., J.Z., and D.L. analyzed the data and wrote the manuscript. D.L. supervised the project. All authors contributed to the manuscript. CRediT: **Chen Li** data curation, investigation; **Jinzhong Zhao** writing-original draft.

Notes

The authors declare no competing financial interest.

■ ACKNOWLEDGMENTS

This work was supported in part by funding from the National Key R&D Program of China (2019YFA0210100) and the National Natural Science Foundation of China (22174072 and 21977053). We are grateful to Professor Ling Huang from our center for his enthusiastic discussion about the data and acknowledge the support from the Fundamental Research Funds for the Central Universities and Frontiers Science Center for Cell Responses, Nankai University.

■ REFERENCES

(1) Leonard, H.; Colodner, R.; Halachmi, S.; Segal, E. Recent Advances in the Race to Design a Rapid Diagnostic Test for Antimicrobial Resistance. *ACS Sens.* **2018**, *3*, 2202−2217.

(2) Li, W.; Wu, G.; Zhang, X.; Yue, A.; Du, W.; Zhao, J.; Liu, D. Research Progress of Bacteria Detection Based on Raman Spectroscopy. *Chem. J. Chin. Univ.* **2020**, *41*, 872−883.

(3) Perez, F.; Bonomo, R. A. Carbapenem-resistant Enterobacteriaceae: global action required. *Lancet Infect. Dis.* **2019**, *19*, 561−562.

(4) Potter, R. F.; D'Souza, A. W.; Dantas, G. The rapid spread of carbapenem-resistant Enterobacteriaceae. *Drug Resistance Updates* **2016**, *29*, 30−46.
(5) Patidar, N.; Vyas, N.; Sharma, S.; Sharma, B. Phenotypic Detection of Carbapenemase Production in Carbapenem-Resistant Enterobacteriaceae by Modified Hodge Test and Modified Strip Carba NP Test. *J. Lab. Physicians* **2021**, *13*, 14−21.
(6) Dubourg, G.; Lamy, B.; Ruimy, R. Rapid phenotypic methods to improve the diagnosis of bacterial bloodstream infections: meeting the challenge to reduce the time to result. *Clin. Microbiol. Infect.* **2018**, *24*, 935−943.
(7) Robinson, C. S.; Timofte, D.; Singer, E. R.; Rimmington, L.; Rubio-Martínez, L. M. Prevalence and antimicrobial susceptibility of bacterial isolates from horses with synovial sepsis: A cross-sectional study of 95 cases. *Vet. J.* **2016**, *216*, 117−121.
(8) Holland, T. L.; Arnold, C.; Fowler, V. G. Clinical management of Staphylococcus aureus bacteremia: a review. *JAMA* **2014**, *312*, 1330−1341.
(9) Burnham, C. D.; Leeds, J.; Nordmann, P.; O'Grady, J.; Patel, J. Diagnosing antimicrobial resistance. *Nat. Rev. Microbiol.* **2017**, *15*, 697−703.
(10) Moniri, A.; Miglietta, L.; Malpartida-Cardenas, K.; Pennisi, I.; Cacho-Soblechero, M.; Moser, N.; Holmes, A.; Georgiou, P.; Rodriguez-Manzano, J. Amplification Curve Analysis: Data-Driven Multiplexing Using Real-Time Digital PCR. *Anal. Chem.* **2020**, *92*, 13134−13143.
(11) Quainoo, S.; Coolen, J. P. M.; van Hijum, S. A. F. T.; Huynen, M. A.; Melchers, W. J. G.; van Schaik, W.; Wertheim, H. F. L. Whole-Genome Sequencing of Bacterial Pathogens: the Future of Nosocomial Outbreak Analysis. *Clin. Microbiol. Rev.* **2017**, *30*, 1015−1063.
(12) Yoon, E. J.; Jeong, S. H. MALDI-TOF Mass Spectrometry Technology as a Tool for the Rapid Diagnosis of Antimicrobial Resistance in Bacteria. *Antibiotics* **2021**, *10*, 982.
(13) Shao, Q.; Zheng, Y.; Dong, X.; Tang, K.; Yan, X.; Xing, B. A covalent reporter of β-lactamase activity for fluorescent imaging and rapid screening of antibiotic-resistant bacteria. *Chem.—Eur. J.* **2013**, *19*, 10903−10910.
(14) Wang, Z.; Xing, B. Small-molecule fluorescent probes: big future for specific bacterial labeling and infection detection. *Chem. Commun.* **2022**, *58*, 155−170.
(15) Shi, H.; Cheng, Y.; Lee, K. H.; Luo, R. F.; Banaei, N.; Rao, J. Engineering the stereochemistry of cephalosporin for specific detection of pathogenic carbapenemase-expressing bacteria. *Angew. Chem., Int. Ed.* **2014**, *53*, 8113−8116.
(16) Mao, W.; Xia, L.; Xie, H. Detection of Carbapenemase-Producing Organisms with a Carbapenem-Based Fluorogenic Probe. *Angew. Chem., Int. Ed.* **2017**, *56*, 4468−4472.
(17) Mao, W.; Wang, Y.; Qian, X.; Xia, L.; Xie, H. A Carbapenem-Based Off-On Fluorescent Probe for Specific Detection of Metallo-β-Lactamase Activities. *ChemBioChem* **2019**, *20*, 511−515.
(18) Wang, J.; Xu, W.; Xue, S.; Yu, T.; Xie, H. A minor structure modification serendipitously leads to a highly carbapenemase-specific fluorogenic probe. *Org. Biomol. Chem.* **2020**, *18*, 4029−4033.
(19) Ma, C. W.; Ng, K. K.; Yam, B. H.; Ho, P. L.; Kao, R. Y.; Yang, D. Rapid Broad Spectrum Detection of Carbapenemases with a Dual Fluorogenic-Colorimetric Probe. *J. Am. Chem. Soc.* **2021**, *143*, 6886−6894.
(20) Das, S.; Ihssen, J.; Wick, L.; Spitz, U.; Shabat, D. Chemiluminescent Carbapenem-based Molecular Probe for Detection of Carbapenemase Activity in Live Bacteria. *Chem.—Eur. J.* **2020**, *26*, 3647−3652.
(21) Zhang, Y.; Lei, J. E.; He, Y.; Yang, J.; Wang, W.; Wasey, A.; Xu, J.; Lin, Y.; Fan, H.; Jing, G.; Zhang, C.; Jin, Y. Label-Free Visualization of Carbapenemase Activity in Living Bacteria. *Angew. Chem., Int. Ed.* **2018**, *57*, 17120−17124.
(22) Longo, G.; Alonso-Sarduy, L.; Rio, L. M.; Bizzini, A.; Trampuz, A.; Notz, J.; Dietler, G.; Kasas, S. Rapid detection of bacterial resistance to antibiotics using AFM cantilevers as nanomechanical sensors. *Nat. Nanotechnol.* **2013**, *8*, 522−526.
(23) Santopolo, G.; Rojo-Molinero, E.; Clemente, A.; Borges, M.; Oliver, A.; de la Rica, R. Bedside Detection of Carbapenemase-Producing Pathogens with Plasmonic Nanosensors. *Sens. Actuators, B* **2021**, *329*, 129059.
(24) Sun, Y.; Zhao, C.; Niu, J.; Ren, J.; Qu, X. Colorimetric Band-aids for Point-of-Care Sensing and Treating Bacterial Infection. *ACS Cent. Sci.* **2020**, *6*, 207−212.
(25) Boehle, K. E.; Gilliand, J.; Wheeldon, C. R.; Holder, A.; Adkins, J. A.; Geiss, B. J.; Ryan, E. P.; Henry, C. S. Utilizing Paper-Based Devices for Antimicrobial-Resistant Bacteria Detection. *Angew. Chem., Int. Ed.* **2017**, *56*, 6886−6890.
(26) Cunningham, S. A.; Limbago, B.; Traczewski, M.; Anderson, K.; Hackel, M.; Hindler, J.; Sahm, D.; Alyanak, E.; Lawsin, A.; Gulvik, C. A.; de Man, T. J. B.; Mandrekar, J. N.; Schuetz, A. N.; Jenkins, S.; Humphries, R.; Palavecino, E.; Vasoo, S.; Patel, R. Multicenter Performance Assessment of Carba NP Test. *J. Clin. Microbiol.* **2017**, *55*, 1954−1960.
(27) Hombach, M.; von Gunten, B.; Castelberg, C.; Bloemberg, G. V. Evaluation of the Rapidec Carba NP Test for Detection of Carbapenemases in Enterobacteriaceae. *J. Clin. Microbiol.* **2015**, *53*, 3828−3833.
(28) Eguchi, M.; Nugraha, A. S.; Rowan, A. E.; Shapter, J.; Yamauchi, Y. Adsorchromism: Molecular Nanoarchitectonics at 2D Nanosheets-Old Chemistry for Advanced Chromism. *Adv. Sci.* **2021**, *8*, 2100539.
(29) Sutton, L. D.; Biedenbach, D. J.; Yen, A.; Jones, R. N. Development, characterization, and initial evaluations of S1 a new chromogenic cephalosporin for β-lactamase delection. *Microbiol. Infect. Dis.* **1995**, *21*, 1−8.
(30) Bush, K. Past and Present Perspectives on β-Lactamases. Antimicrob. *Agents Chemother.* **2018**, *62*, 010766.
(31) *English Surveillance Programme for Antimicrobial Utilisation and Resistance (ESPAUR)*; Public Health England: London, 2018.
(32) Meredith, H. R.; Andreani, V.; Ma, H. R.; Lopatkin, A. J.; Lee, A. J.; Anderson, D. J.; Batt, G.; You, L. Applying ecological resistance and resilience to dissect bacterial antibiotic responses. *Sci. Adv.* **2018**, *4*, No. eaau1873.
(33) Rubtsova, M. Y.; Ulyashova, M. M.; Edelstein, M. V.; Egorov, A. M. Oligonucleotide microarrays with horseradish peroxidase-based detection for the identification of extended-spectrum β-lactamases. *Biosens. Bioelectron.* **2010**, *26*, 1252−1260.
(34) Tamma, P. D.; Doi, Y.; Bonomo, R. A.; Johnson, J. K.; Simner, P. J.; Tamma, P. D.; Doi, Y.; Bonomo, R. A. Antibacterial Resistance Leadership Group. A Primer on AmpC β-Lactamases: Necessary Knowledge for an Increasingly Multidrug-resistant World. *Clin. Infect. Dis.* **2019**, *69*, 1446−1455.
(35) Modi, T.; Risso, V. A.; Martinez-Rodriguez, S.; Gavira, J. A.; Mebrat, M. D.; Van Horn, W. D.; Sanchez-Ruiz, J. M.; Banu Ozkan, S. Hinge-shift mechanism as a protein design principle for the evolution of β-lactamases from substrate promiscuity to specificity. *Nat. Commun.* **2021**, *12*, 1852.
(36) van Zundert, G. C. P.; Rodrigues, J. P. G. L. M.; Trellet, M.; Schmitz, C.; Kastritis, P. L.; Karaca, E.; Melquiond, A. S. J.; van Dijk, M.; de Vries, S. J.; Bonvin, A. M. J. J. The HADDOCK2.2 Web Server: User-Friendly Integrative Modeling of Biomolecular Complexes. *J. Mol. Biol.* **2016**, *428*, 720−725.
(37) Vangone, A.; Bonvin, A. M. Contacts-based prediction of binding affinity in protein-protein complexes. *Elife* **2015**, *4*, No. e07454.
(38) Xue, L. C.; Rodrigues, J. P.; Kastritis, P. L.; Bonvin, A. M.; Vangone, A. PRODIGY: a web server for predicting the binding affinity of protein-protein complexes. *Bioinformatics* **2016**, *32*, 3676−3678.
(39) *CLSI Performance Standards for Antimicrobial Susceptibility Testing*, 29th ed.; Clinical and Laboratory Institute: Wayne, 2019.
(40) Routsias, J. G.; Tsakogiannis, D.; Katsiki, M.; Marinou, D.; Mavrouli, M.; Vrioni, G.; Tsakris, A. Development of a new

https://doi.org/10.1021/jacsau.2c00607
JACS Au 2023, 3, 227−238

spectrophotometric assay for rapid detection and differentiation of KPC, MBL, and OXA-48 carbapenemase-producing Klebsiella pneumoniae clinical isolates. *Int. J. Antimicrob. Agents* **2020**, *56*, 106211.
(41) Gill, C. M.; Lasko, M. J.; Asempa, T. E.; Nicolau, D. P. Evaluation of the EDTA-Modified Carbapenem Inactivation Method for Detecting Metallo-β-Lactamase-Producing Pseudomonas aeruginosa. *J. Clin. Microbiol.* **2020**, *58*, e02015−e02019.
(42) Stojanoski, V.; Chow, D. C.; Fryszczyn, B.; Hu, L.; Nordmann, P.; Poirel, L.; Sankaran, B.; Prasad, B. V.; Palzkill, T. Structural Basis for Different Substrate Profiles of Two Closely Related Class D β-Lactamases and Their Inhibition by Halogens. *Biochemistry* **2015**, *54*, 3370−3380.
(43) Kaukonen, K. M.; Bailey, M.; Suzuki, S.; Pilcher, D.; Bellomo, R. Mortality related to severe sepsis and septic shock among critically Ill patients in Australia and New Zealand, 2000−2012. *JAMA* **2014**, *311*, 1308−1316.
(44) Gyawali, B.; Ramakrishna, K.; Dhamoon, A. S. Sepsis: The evolution in definition, pathophysiology, and management. *SAGE Open Med.* **2019**, *7*, 2050312119835043.
(45) Puskarich, M. A.; Trzeciak, S.; Shapiro, N. I.; Heffner, A. C.; Kline, J. A.; Jones, A. E. Outcomes of patients undergoing early sepsis resuscitation for cryptic shock compared with overt shock. *Resuscitation* **2011**, *82*, 1289−1293.
(46) Mayr, F. B.; Yende, S.; Angus, D. C. Epidemiology of severe sepsis. *Virulence* **2014**, *5*, 4−11.
(47) Martinez, A. W.; Phillips, S. T.; Butte, M. J.; Whitesides, G. M. Patterned Paper as a Platform for Inexpensive, Low-Volume, Portable Bioassays. *Angew. Chem., Int. Ed.* **2007**, *46*, 1318−1320.
(48) Cate, D. M.; Adkins, J. A.; Mettakoonpitak, J.; Henry, C. S. Recent Developments in Paper-Based Microfluidic Devices. *Anal. Chem.* **2015**, *87*, 19−41.
(49) Baş, D. Sensitive and reliable paper-based glucose sensing mechanisms with smartphone readout using the L*a*b* color space. *Anal. Methods* **2017**, *9*, 6698−6704.
(50) Rees, C. A.; Nasir, M.; Smolinska, A.; Lewis, A. E.; Kane, K. R.; Kossmann, S. E.; Sezer, O.; Zucchi, P. C.; Doi, Y.; Hirsch, E. B.; Hill, J. E. Detection of high-risk carbapenem-resistant Klebsiella pneumoniae and Enterobacter cloacae isolates using volatile molecular profiles. *Sci. Rep.* **2018**, *8*, 13297.
(51) *CLSI Performance Standards for Antimicrobial Susceptibility Testing*, 20th ed.; Clinical and Laboratory Institute: Wayne, 2018.
(52) Pierce, V. M.; Simner, P. J.; Lonsway, D. R.; Roe-Carpenter, D. E.; Johnson, J. K.; Brasso, W. B.; Bobenchik, A. M.; Lockett, Z. C.; Charnot-Katsikas, A.; Ferraro, M. J.; Thomson, R. B.; Jenkins, S. G.; Limbago, B. M.; Das, S. Modified Carbapenem Inactivation Method for Phenotypic Detection of Carbapenemase Production among Enterobacteriaceae. *J. Clin. Microbiol.* **2017**, *55*, 2321−2333.

https://doi.org/10.1021/jacsau.2c00607
JACS Au 2023, 3, 227−238